Analysis of Light Transport in Scattering Media

Yasuhiro Mukaigawa[1,2]   Yasushi Yagi[1]   Ramesh Raskar[2]

[1]Osaka University   [2]MIT Media Lab

Abstract

We propose a new method to analyze light transport in homogeneous scattering media. The incident light undergoes multiple bounces in translucent objects, and produces a complex light field. Our method analyzes the light transport in two steps. First, single and multiple scattering are separated by projecting high-frequency stripe patterns. Then, multiple scattering is decomposed into each bounce component based on the light transport equation. The light field for each bounce is recursively estimated. Experimental results show that light transport in scattering media can be decomposed and visualized for each bounce.

1. Introduction

Most objects in our everyday environment are not perfectly opaque, but translucent. Although marble, skin, and milk are considered typical translucent objects, there are many more such objects including fruit and vegetables. In translucent objects, an incident ray undergoes repeated scattering, and results in a complex light field. However, we cannot directly measure the light field within a scattering material. Understanding how an incident ray repeats scattering and the light propagates in a scattering media is fundamental for many applications such as rendering, medical imaging, and material estimation.

Several methods have been proposed to analyze single scattering in *optically thin media* such as fog or underwater. Narasimhan et al. [1] estimated scattering parameters of diluted homogeneous liquid. Gu et al. [2] recovered inhomogeneous participating media by projecting structured light. Hawkins et al. [3] estimated time-varying density of smoke by scanning laser. These methods give good results because a ray from light source bounces only once in the media and the path of the ray is simply estimated as shown Fig. 1(a) . These methods can analyze only *single scattering in optically thin media*.

To deal with *optically dense media*, the spatial distribution of multiple scattering should be modeled. It is well known that light distribution in dense media becomes

(a) single scattering

(b) diffusion approximation
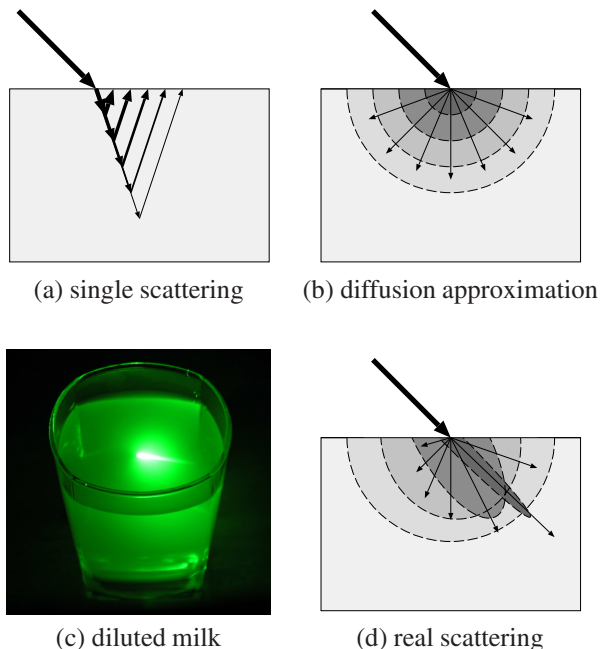

(c) diluted milk

(d) real scattering

Figure 1. Distribution of scattering lights in the media.

isotropic after incident rays undergo scattering many times as shown Fig. 1(b). This is called *diffusion approximation*. Stam [4] approximated the effects of multiple scattering in heterogeneous media. Jensen et al. [5] proposed an analytic dipole model based on the diffusion approximation. Donner [6] further extended this by a multipole diffusion approximation to render thin translucent slabs. However, these methods cannot analyze anisotropic distribution of lower-order scattering such as 2- and 3-bounce scattering.

Recently, Donner et al. [7] presented an empirical BSS-RDF model to express directionally-dependent distribution. For example, Fig. 1(c) shows diluted milk illuminated by green laser illumination. Both single and multiple scattering are observed, and they generate a complex light field as shown in Fig. 1(d). To handle this kind of general translucent objects, the light transport for each bounce should be separately analyzed. Seitz et al. [12] proposed *inverse light transport* to decompose inter-reflections on the surface into

each bounce component.

Our contribution is similar to the inverse light transport, but we aim to decompose scattering light in translucent volumetric media. Although our method assumes that the target object is a low-height 2-D volume and homogeneous for simplification, directionally-dependent distribution can be analyzed in detail by tracing multi-bounce scattering light. This paper introduces a new approach to recursively predict the higher-order bounce scattering based on the *light transport equation*.

2. Related work

Analysis based on dipole model: Since the dipole model can express isotropic distribution of multiple scattering with a simple equation, it is used not only for rendering but also image analysis. As illumination, arbitrary light environment [8], a focused narrow beam using a lens [5], a sweeping laser beam [9], a projector [10], or a fiber optic spectrometer [11] are used to capture image, and the dipole model is fit. These methods can be applied only for optically dense media.

Face: Skin translucency has been the focus of much research. Tsumura [13] proposed a method to separate the hemoglobin and melanin components by independent component analysis, and estimated irradiance by the deconvolution of the point spread function of translucent media [14]. More recently, the layered structure of skin has been analyzed and used for photo-realistic rendering [15] [16].

Medical imaging: Interestingly, tomography in medical imaging deals with similar scattering problems [17][18]. Computational Tomography (CT) using x-rays can avoid most difficulties associated with light diffusion because x-rays go through the body without scattering. On the other hand, Diffuse Optical Tomography (DOT) using near-infrared light assumes that incident light diffuses in the body. Almost all DOT techniques assume that the diffusion is isotropic. Only a few methods attempt to use directionally-dependent distribution models based on the transport equation [19].

3. Light transport model in scattering media

3.1. Ray scattering

In a scattering media, the power of a ray is attenuated by repeating scattering. First, we have to model the attenuation of the scattering. Figure 2 illustrates a simple path of a ray emitted from a point p_1, scattered at a point p_2, and finally reaching at a point p_3. According to the participating media theory [4], the power of the ray l_{p_3} at the point p_3 can be modeled as

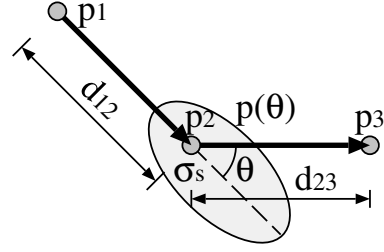$$l_{p_3} = l_{p_1} \sigma_s p(\theta) e^{-\sigma_t (d_{12}+d_{23})}. \tag{1}$$

Figure 2. Scattering model.

Here, l_{p_1} is the power of the ray at the point p_1. σ_s and σ_t are scattering and extinction coefficients of the media. d_{12} and d_{23} are distances from p_1 to p_2 and from p_2 to p_3, respectively. The phase function $p(\theta)$ defines asymmetry of the scattering distribution, and it is approximated by

$$p(\theta) = \frac{1}{4\pi} \frac{1 - g^2}{(1 + g^2 - 2g\cos\theta)^{\frac{3}{2}}}. \tag{2}$$

The parameter g controls the shape of the distribution.

3.2. Component of light field

The power distribution of all rays for each position and for each direction is expressed by a light field L. The light field can be decomposed into each bounce component. Let's assume that L_0 is the light field directly generated by a light source. In a scattering media, L_0 is scattered once and generates 1-bounce light field L_1. The 1-bounce scattering is called *single scattering*. Then the 1-bounce light field acts as an illumination and generates 2-bounce light field L_2. Similarly, k-bounce light field L_k generates $(k+1)$-bounce light field L_{k+1}. The 2- or higher-order bounce scattering is called *multiple scattering*. The complete light field in the media is expressed as a sum of each bounce component by

$$L = \sum_{k=1}^{\infty} L_k. \tag{3}$$

The light transport in the media is expressed by a light transport matrix T. The matrix describes how a ray from a point is propagated to other points, and can be calculated by Eq.(1), if parameters of the scattering media are known. By the light transport matrix, the 1-bounce light field corresponding to single scattering is expressed as $L_1 = TL_0$. The 2-bounce light field is expressed as $L_2 = TL_1$. Similarly, the k-bounce light field is expressed recursively by

$$L_k = TL_{k-1}. \tag{4}$$

3.3. Dimension of light field

Now, we define a concrete description of the light field. The light field in a volume can be expressed as a 4-D func-
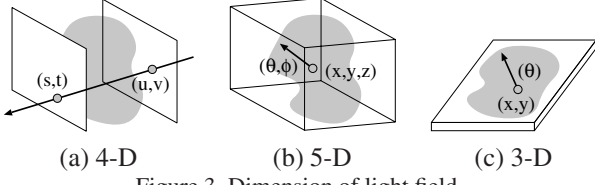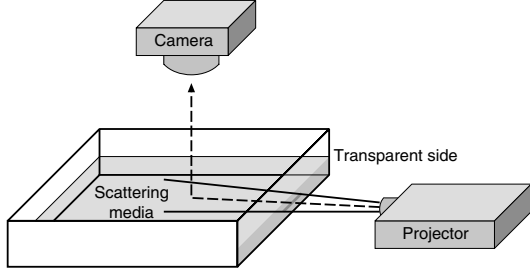
(a) 4-D   (b) 5-D   (c) 3-D

Figure 3. Dimension of light field.

Figure 4. Placement of the camera and projector.

Figure 5. Light field and observed image.

tion. Two parallel planes sandwiching the volume define all rays by two coordinates (u, v) and (s, t) as shown in Fig. 3(a). However, this definition assumes that the space is vacuum and the power of the rays does not change along the path.

In the scattering media, the power of rays attenuates along the path. Hence, the light field should be expressed as a 5-D function of the point (x, y, z) and the direction (θ, ϕ) as shown in Fig. 3(b). In general, the 5-D light field is hard to handle and visualize because the data size becomes extremely large.

If we limit the shape of the target object to low-height volume like a plate, the light field can be expressed as a 3-D function $l(x, y, \theta)$ of the point (x, y) and the direction (θ). The light field vector L is defined as a series of the function as

$$L = [l(0, 0, 0), \cdots, l(W, H, 2\pi)]^T. \quad (5)$$

Here, W and H denote the width and height of the media, respectively.

In this paper, we assume a 2-D volume and a 3-D light field function, and fully analyze the light transport in scattering media.

3.4. Light field and observed image

We assume that a camera observes intensities over the surface of the target 2-D volume as shown in Fig. 4, and captures an image I. The image I can be decomposed into individual bounce scattering as
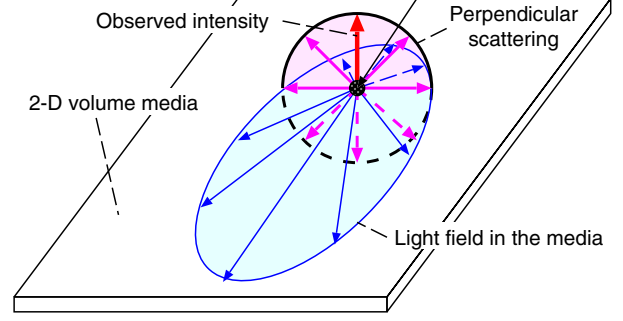
$$I = \sum_{k=1}^{\infty} I_k. \quad (6)$$

However, each bounce image I_k is not a slice of the corresponding light field L_k. While the light field describes the distribution of the rays in the 2-D volume media, the observed image is a collection of rays of the surface normal direction as shown in Fig. 5.

To associate the light field with the observed image, we utilize the *rotational symmetry* of the scattering light around the ray. The power of the scattering light in the perpendicular directions is uniform regardless of the rotational direction. That is, the observed intensities in the image are equal to power of the scattered ray calculated by Eq. (1) with $\theta = \pi/2$. Hence, the k-bounce light field L_k and the light transport matrix T can predict both L_{k+1} and I_{k+1}.

4. Analysis of light transport

4.1. Flow of the process

The incident light to a translucent object repeats scattering in the media, and generates a complex light field. Our goal is to visualize how the incident light propagates in scattering media by tracing its light transport and decomposing the light field for each bounce.

Figure 6 summarize the flow of analysis. First, single and multiple scattering are separated by projecting high-frequency stripe patterns. Then, the extinction parameter σ_t is estimated from the separated pure single scattering image. Then, multiple scattering is predicted from the light field of the single scattering with changing parameters. Thus, the light field is decomposed for each bounce scattering. In the following three sections, the detailed algorithms are described.

4.2. Separation of single and multiple scattering

All the bounce components are mixed in a captured image. Since each component has its own spatial distribution, direct analysis of the mixed components is not easy. Hence, we propose a new method to separate single and multiple scattering using a projector.
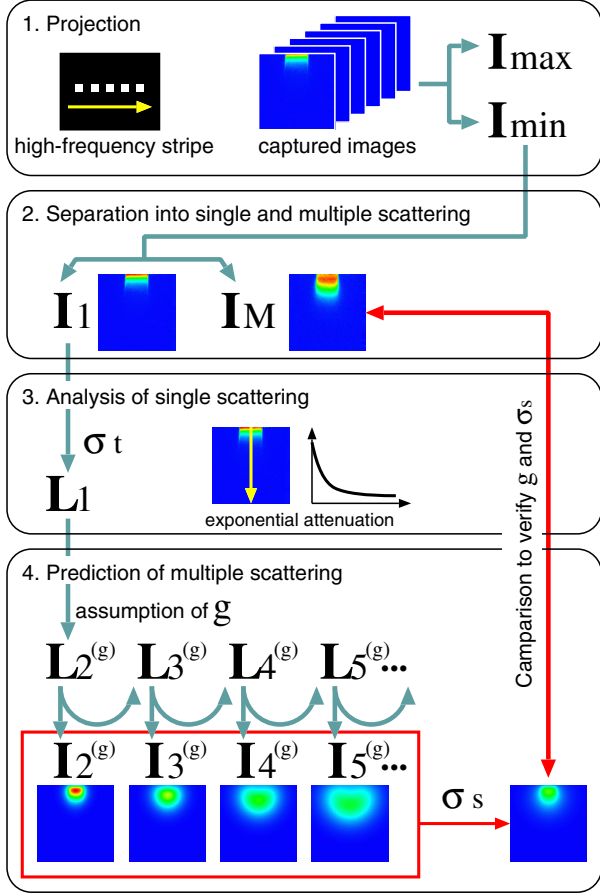
Figure 6. Flow of analysis. Scattering parameters (σ_t, σ_s, and g) are sequentially estimated.
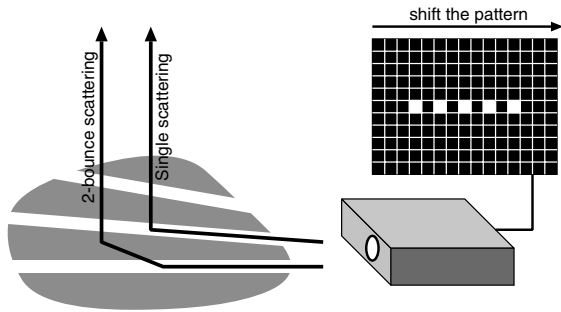

Figure 7. Pattern projection of High-frequency stripes. By shifting the stripes, single and multiple scattering are separated.

Nayar et al. [20] presented an effective method to separate direct and global component by projecting 2-D high-frequency patterns on the target scene. In their original method, the direct component corresponds to diffuse and specular reflections, and the global component corresponds to indirect reflections such as inter-reflection.

Since we want to separate single and multiple scattering,

we change the projecting patterns to 1-D high-frequency stripes with alternate white and black pixels as shown in Fig. 7. In this case, single scattering is the direct component because single scattering is caused by 1-bounce in the media. Multiple scattering is the global component because it is observed regardless of the direct illumination from the projector.

By shifting the 1-D high-frequency stripe pattern, several images are captured. The maximum and minimum intensities are found for each pixel to generate images I_{max} and I_{min} which has the maximum and minimum intensities, respectively. Then, a single scattering image I_1 and a multiple scattering image I_M which corresponds to $\sum_{k=2}^{\infty} I_k$ are calculated by [20]

$$I_1 = I_{max} - I_{min}, \qquad (7)$$
$$I_M = 2I_{min}. \qquad (8)$$

This allows us to easily separate single and multiple scattering.

4.3. Analysis of single scattering

The single scattering is caused by one bounce of a ray between the light source and the camera. Therefore, the path of the ray is easily traced. Since the power of the light exponentially attenuates along the path, we fit an exponential function.

Let $s(d)$ be the intensity of I_1 at the distance d from the incident point. Then, the extinction coefficient σ_t is estimated so that the error between an exponential function and $s(d)$ becomes minimum by

$$\arg\min_{c,\sigma_t} ||s(d) - ce^{-\sigma_t d}||_2 \qquad (9)$$

Here, c is a scale parameter of the exponential function.

The light field L_1 caused by the single scattering is simple because rays from the light source go straight in the media with exponentially attenuating the power. Hence, L_1 is easily estimated up to scale factor.

4.4. Analysis of multiple scattering

Next, we recursively estimate the higher-order light fields corresponding to multiple scattering. At this point, the asymmetric parameter g and scattering coefficient σ_s are unknown. We estimate these parameters based on the forward rendering process. However, our forward rendering is a unique two-step process that is optimized for bounce analysis.

In the first step, we render each bounce component separately without deciding the parameter σ_s. We temporarily assume $\sigma_s = 1$. Since the range of the asymmetric parameter is limited by $-1 \le g \le 1$, some candidates of the 2-bounce light field $L_2^{(g)}$ can be generated with changing the
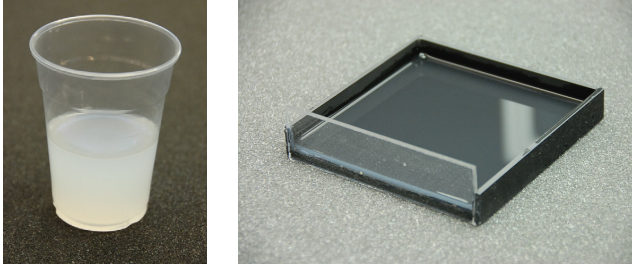
(a) Diluted milk   (b) Case for measurement

Figure 8. Target scattering media.

parameter g. The higher-order (k-bounce) light fields $\boldsymbol{L}_k^{(g)}$ and the corresponding images $\boldsymbol{I}_k^{(g)}$ are recursively rendered according to the light transport equation of Eq. (1).

In the second step, the asymmetric parameter g and scattering coefficient σ_s are found so that the estimated higher-order component fits the real multiple scattering component $\boldsymbol{I}_M$ separated in section 4.2. The concrete error is defined by

$$\arg\min_{\sigma_s, g} ||\boldsymbol{I}_M - \sum_{k=2}^{\infty} \sigma_s^{k-1} \boldsymbol{I}_k^{(g)}||_2. \qquad (10)$$

It is noted that σ_s does not affect the image $\boldsymbol{I}_k^{(g)}$ and light field $\boldsymbol{L}_k^{(g)}$, and is only used as the weight of the linear combination of each bounce. Hence, two parameters are efficiently estimated without changing them simultaneously.

Then, the complete light field $\boldsymbol{L}$ is expressed as a linear combination of each bounce component by

$$\boldsymbol{L} = \sum_{k=1}^{\infty} \sigma_s^{k-1} \boldsymbol{L}_k. \qquad (11)$$

This analysis gives us the decomposed light fields and the light transport in the scattering media.

This idea of two-step rendering is useful because the parameter σ_s can be easily changed after the first step via relatively simple and fast linear combination of bounce component images. Computer graphics rendering methods do not allow post-synthesis parameter manipulation. We render each bounce independently which means we can easily modify the parameter via linear combination.

5. Experiment

5.1. Setup

We show some experimental results of light transport analysis of real material. We used diluted milk with water as scattering media as shown in Fig. 8 (a) so that both single and multiple scattering are observed. The liquid is poured into the case painted with matte black. The height of the liquid is less than 5mm. Only one single side of the
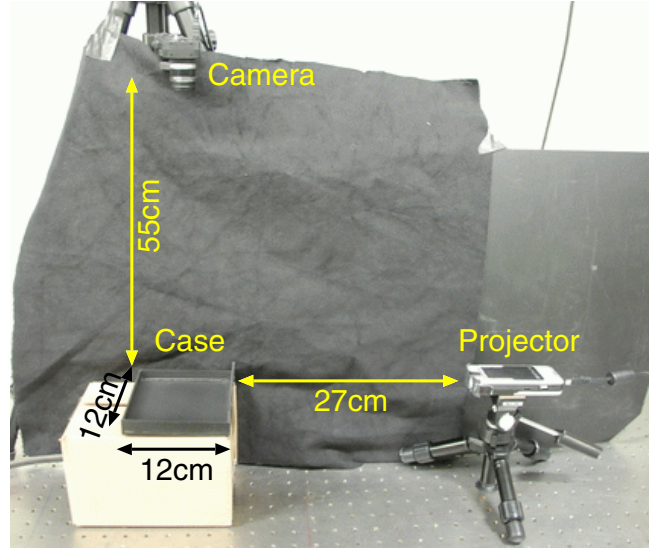

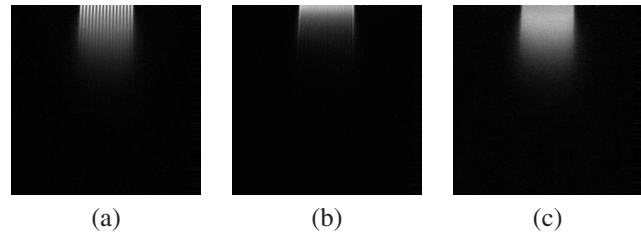Figure 9. Setup for measurement.

(a)   (b)   (c)

Figure 10. Separation of single and multiple scattering components. (a) one of the captured images under the high-frequency stripe illumination. (b) separated single scattering. (c) separated multiple scattering

case is transparent so that the liquid can be illuminated from the side as shown in (b).

Figure 9 shows the setup for measurement. A 3M MPro110 projector is located to illuminate the liquid in the case from the side, and a Point Grey Chameleon camera is located at the top to capture images from normal direction of the target plane.

5.2. Separation of single and multiple scattering

First, single and multiple scattering are separated. Six images are captured with shifting the high-frequency stripe pattern. Figure 10 (a) shows one of the captured images. The separated results are shown in (b) and (c).

To evaluate accuracy of the separated single scattering component, we compared the attenuation of the original intensity without separation and the single scattering obtained by separation. Figure 11 shows how the incident light attenuates with distance from the incident point. The red lines show the real attenuation, and the blue lines show the fit-
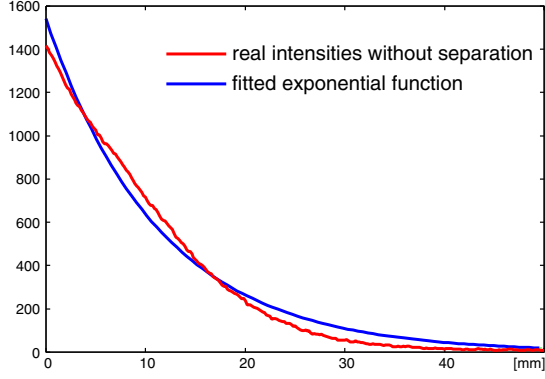
(a) without separation
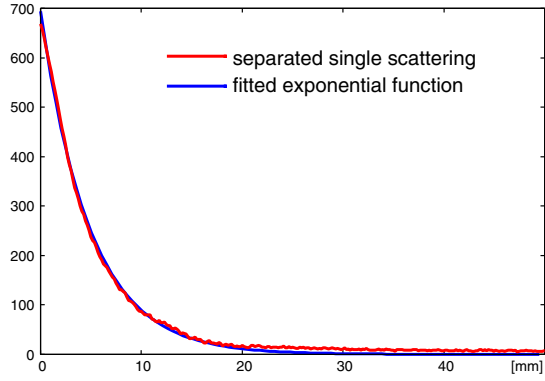
(b) single scattering

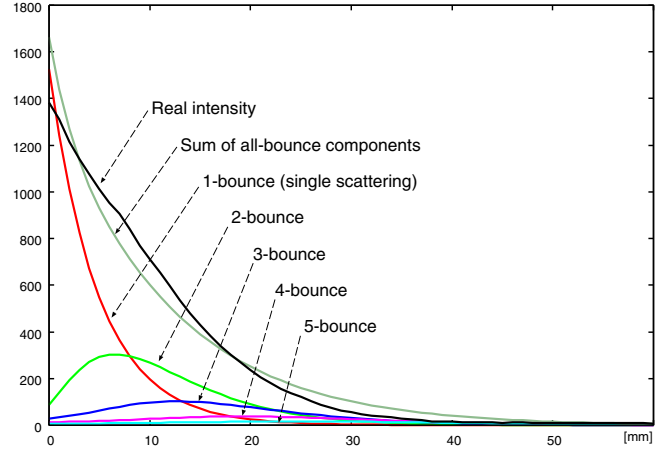Figure 11. Attenuation of incident illumination.

Figure 12. Decomposition of multiple scattering. Real intensities are decomposed into each bounce scattering component. Higher-order components have peaks in the media and the peak positions move inside as the bounce order becomes higher.

(a) Real intensity (b) Estimated light field

(c) 1-bounce (d) 2-bounce

(e) 3-bounce (f) 4-bounce

(g) 5-bounce (h) 6-bounce

Figure 13. Decomposed light field. The distribution of the lower-order bounce component have directional properties while the distribution becomes isotropic as the bounce order becomes higher.

ting results of the exponential function. We can see that the exponential function does not fit original intensity because it contains a lot of higher-order scattering components. On the other hand, the exponential function well fits the single scattering component. We can see that the separated single scattering matches the light transport model and that extinction coefficient can be effectively estimated. From this result, the value of σ_t was estimated as 0.2051, and the light field of the single scattering was obtained.

5.3. Decomposition of light field

Next, the most appropriate parameter set ($\sigma_a = 0.0366$ and $g = 0.4$) are estimated and the higher-order bounce components are recursively calculated. Figure 12 shows how the incident light attenuates with distance from the incident point for each bounce component. We can see that the single scattering has a peak at the incident point and exponentially attenuates, while higher-order components have peaks in the media, and the peak positions move inside as the bounce order becomes higher.

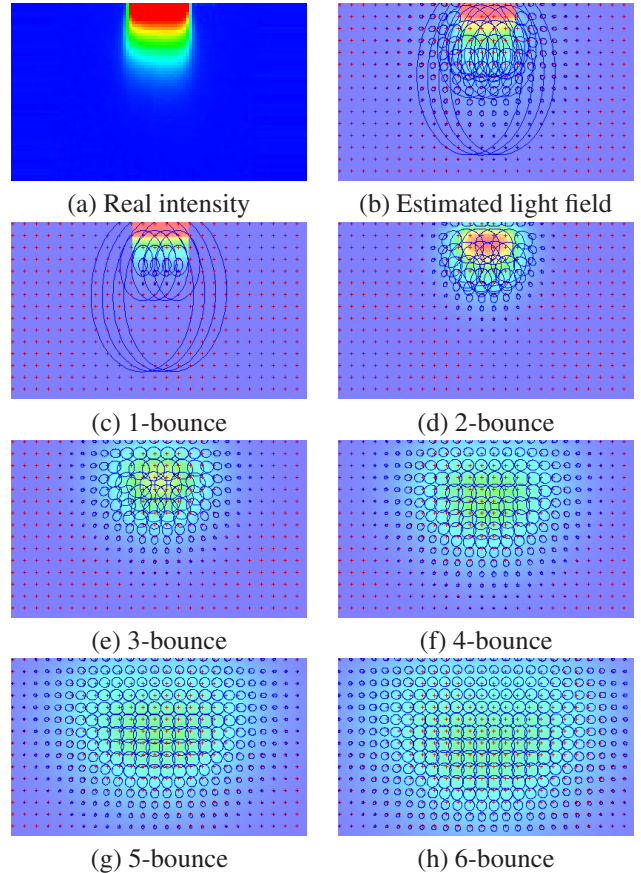Finally, the light fields for each bounce component are obtained as shown in Fig.13. In this figure, the intensities are expressed in pseudo-color, while red '+' markers indi-

(a) Real intensity   (b) Estimated light field

(c) 1-bounce   (d) 2-bounce

(e) 3-bounce   (f) 4-bounce
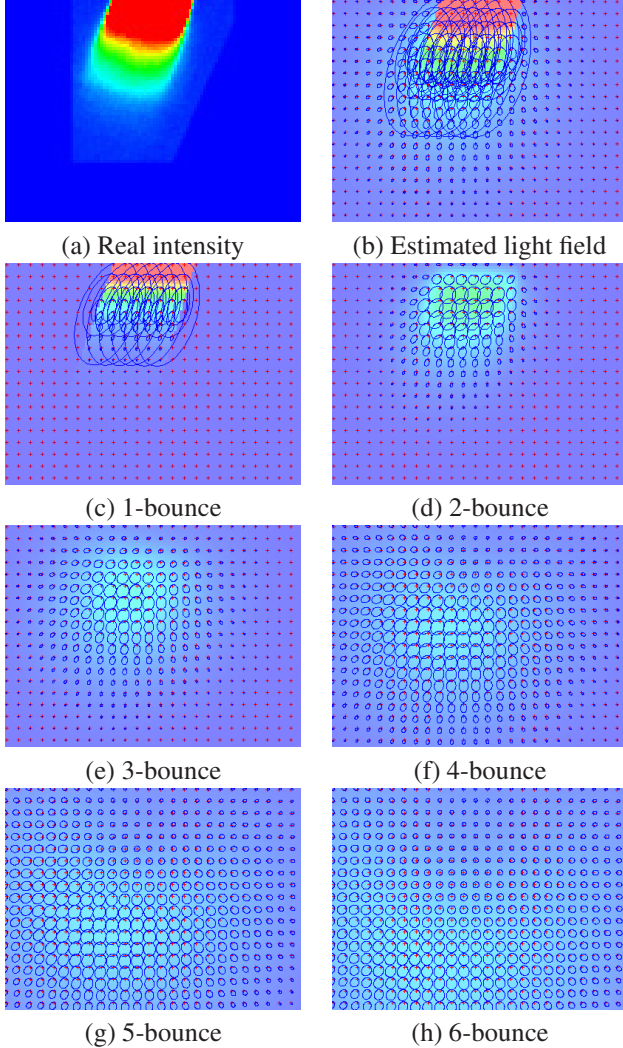
(g) 5-bounce   (h) 6-bounce

Figure 14. Light fields of the slant incident illumination. The difference of directive properties are clearly observed.

cate the sampling points and blue ellipses indicate the angular distributions of the light field at the sampling point. We can see that the distribution of the lower-order bounce component have directional characteristics while the distribution becomes isotropic as the bounce order becomes higher. These visualizations show how the incident ray repeats scattering and the light is transported in the scattering media.

Figure 14 shows another results that incident angle s slant. The direction of single scattering is same as the incident angle, the direction of 2-bounce scattering is weakly affected by the incident angle. The higher-order scattering becomes almost isotropic regardless of the incident angle.

6. Limitation

3-D light field: We assume that the target material has a low-height and the light field is described as a 3-D function. If the target object is a 3-D volume, analysis, storage, and visualization become difficult.

Homogeneous material: Our method assumes that the scattering properties are uniform over the material. If the material is inhomogeneous, the light source should be moved to get more images like CT.

Computational cost: In our method, scattering parameters are estimated within one second. However, the recursive calculation of light field by Eq. (4) requires several hours because all rays were traced exhaustively. To shorten the computational time, some fast methods such as Monte Carlo sampling may be applied.

7. Conclusion

We propose a new method to decompose light field for each bounce and visualize the light transport in a scattering media. Multi bounce scattering is effectively analyzed by two steps. First, single and multiple scattering are separated by projecting 1-D high-frequency stripe patterns. From the pure single scattering, the property of attenuation is stably estimated. Then, multiple scattering is recursively decomposed into each bounce component based on the light transport equation. Although the target object is limited to low-height, we believe that our method is a significant first step in analyzing light transport in translucent objects.

Our future work is verification of the decomposed light transport. Since we do not know the ground truth, we did not compare the results. We are planning to find relationship of the density of the liquid and the estimated parameters. To estimate spatial distribution of the scattering parameters is also our future work, so that inhomogeneous material can be analyzed. Since the number of unknowns increases, we may have to capture multiple images with changing illumination.

Acknowledgment

References

[1] S. G. Narasimhan, M. Gupta, C. Donner, R. Ramamoorthi, S. K. Nayar,, and H. W. Jensen, "Acquiring scattering properties of participating media by dilution", Proc. SIGGRAPH2006, pp.1003-1012, 2006.

[2] J. Gu, S. K. Nayar, E. Grinspun, P. N. Belhumeur and R. Ramamoorthi, "Compressive Structured Light for Re-

covering Inhomogeneous Participating Media", Proc. ECCV2008, pp.845-858, 2008.

[3] T. Hawkins, P. Einarsson, and P. Debevec, "Acquisition of Time-Varying Participating Media", Proc. SIGGRAPH2005, pp.812-815, 2005.

[4] J. Stam, "Multiple scattering as a diffusion process", Proc. Eurographics Rendering Workshop, 1995.

[5] H. W. Jensen, S. R. Marschner, M. Levoy, and P. Hanrahan, "A Practical Model for Subsurface Light Transport", Proc. SIGGRAPH2001, pp.511-518, 2001.

[6] C. Donner H. W. Jensen, "Light Diffusion in Multi-Layered Translucent Materials", Proc. SIGGRAPH2005, pp.1032-1039, 2005.

[7] C. Donner, J. Lawrence, R. Ramamoorthi, T. Hachisuka, H. W. Jensen, and S. Nayar, "An empirical BSSRDF model", Proc. SIGGRAPH2009, pp.1-10, 2009.

[8] Y. Mukaigawa, K. Suzuki, and Y. Yagi, "Analysis of Subsurface Scattering based on Dipole Approximation", IPSJ TCVA, Vol.1, pp.128-138, 2009.

[9] M. Goesele, H. P. A. Lensch, J. Lang, C. Fuchs, and H. P. Seidel, "Disco - Acquisition of Translucent Objects", Proc. SIGGRAPH2004, pp.835-844, 2004.

[10] S. Tariq, A. Gardner, I. Llamas, A. Jones, P. Debevec, and G. Turk, "Efficient Estimation of Spatially Varying Subsurface Scattering Parameters", Vision, Modeling, and Visualization (VMV2006), 2006.

[11] T. Weyrich, W. Matusik, H. Pfister, B. Bickel, C. Donner, C. Tu, J. McAndless, J. Lee, A. Ngan, H. W. Jensen, and M. Gross, "Analysis of Human Faces using a Measurement-Based Skin Reflectance Model", Proc. SIGGRAPH2006, pp.1013-1024, 2006.

[12] S. M. Seitz, Y. Matsushita, and K. N. Kutulakos, "A Theory of Inverse Light Transport", Proc. ICCV2005, pp.1440-1447, 2005.

[13] N. Tsumura, N. Ojima, K. Sato, M. Shiraishi, H. Shimizu, H. Nabeshima, S. Akazaki, K. Hori, and Y. Miyake, "Image-based skin color and texture analysis/synthesis by extracting hemoglobin and melanin information in the skin", Proc. SIGGRAPH2003, pp.770-779, 2003.

[14] N. Tsumura, R. Usuba, K. Takase, T. Nakaguchi, N. Ojima, N. Komeda, and Y. Miyake, "Image-based control of skin translucency", Proc. CGIV2006, pp. 8-11, 2006.

[15] A. Ghosh, T. Hawkins, P. Peers, S. Frederiksen, and P. Debevec, "Practical Modeling and Acquisition of Layered Facial Reflectance", Proc. SIGGRAPH Asia 2008.

[16] C. Donner, T. Weyrich, E. d'Eon, R. Ramamoorthi, S. Rusinkiewicz, "A Layered, Heterogeneous Reflectance Model for Acquiring and Rendering Human Skin", Proc. SIGGRAPH Asia 2008.

[17] D. A. Boas, D. H. Brooks, E. L. Miller, C. A. DiMarzio, M. Kilmer, R. J. Gaudette, and Q. Zhang, "Imaging the body with diffuse optical tomography", IEEE Signal Processing Magazine, Vol.18, Issue 6, pp.57-75, 2001.

[18] A. P. Gibson, J. C. Hebden, and S. R. Arridge, "Recent advances in diffuse optical imaging", Phys. Med. Biol. 50, R1-R43, 2005.

[19] A. D. Klose and A. H. Hielscher, "Iterative reconstruction scheme for optical tomography based on the equation of radiative transfer", Med. Phys. Vol.26, Issue 8, pp.1698-1707, 1999.

[20] S. K. Nayar, G. Krishnan, M. D. Grossberg, and R. Raskar, "Fast Separation of Direct and Global Components of a Scene using High Frequency Illumination", Proc. SIGGRAPH2006, pp.935-944, 2006.